Transport coefficient sensitivities in a semi-analytic model for magnetized liner inertial fusion

Y. Lawrence ; J. R. Davies ; R. D. McBride ; A. B. Sefkow ✉

Check for updates

View Online

Export Citation

Articles You May Be Interested In

Transport coefficients for magnetic-field evolution in inviscid magnetohydrodynamics

Phys. Plasmas (January 2021)

The effect of laser entrance hole foil thickness on MagLIF-relevant laser preheat

Phys. Plasmas (November 2020)

Impact of electron transport models on capillary discharge plasmas

Phys. Plasmas (June 2022)

22 November 2024 21:39:52

Physics of Plasmas

Special Topics Open for Submissions

Learn More

Transport coefficient sensitivities in a semi-analytic model for magnetized liner inertial fusion

Y. Lawrence,[1] (iD) J. R. Davies,[2,3] (iD) R. D. McBride,[4] (iD) and A. B. Sefkow[2,3,5,6,a] (iD)

AFFILIATIONS

[1]Plasma Science & Fusion Center, Massachusetts Institute of Technology, Cambridge, Massachusetts 02139, USA
[2]Laboratory for Laser Energetics, University of Rochester, Rochester, New York 14623, USA
[3]Department of Mechanical Engineering, University of Rochester, Rochester, New York 14627, USA
[4]Department of Nuclear Engineering and Radiological Sciences, University of Michigan, Ann Arbor, Michigan 48109, USA
[5]Department of Physics, University of Rochester, Rochester, New York 14627, USA
[6]Department of Computer Science, University of Rochester, Rochester, New York 14627, USA

[a]Author to whom correspondence should be addressed: adam.sefkow@rochester.edu

ABSTRACT

Performance of magnetized liner inertial fusion (MagLIF) experiments is highly dependent on transport processes including magnetized heat flows and magnetic flux losses. Magnetohydrodynamic simulations used to model these experiments require a choice of model for the transport coefficients, which are the constants of proportionality relating driving terms, such as temperature gradients and currents, to the associated heat and magnetic field transport. The coefficients have been the subject of repeated recalculation using various methods throughout the years. Using a semi-analytic MagLIF model [McBride and Slutz, Phys. Plasmas **22**, 052708 (2015)], we compare models for the transport coefficients provided by Braginskii [*Reviews of Plasma Physics*, edited by M. A. Leontovich (Consultants Bureau, New York, 1965), Vol. 1, p. 205], Epperlein and Haines [Phys. Fluids **29**, 1029 (1986)], Ji and Held [Phys. Plasmas **20**, 042114 (2013)], Davies *et al.* [Phys. Plasmas **28**, 012305 (2021)], and Sadler *et al.* [Phys. Rev. Lett. **126**, 075001 (2021)]. The choice of model modifies magnetic-flux losses caused by the Nernst thermoelectric effect and thermal conduction losses. We present simulated results from parameter scans conducted in order to compare the effects of the different models on parameters of interest in MagLIF. In some regions of parameter space, discrepancies of up to 38% are found in integrated quantities like the fusion yield. These results may serve as a guide for experimental validation of the various models, particularly as laser preheat energies and initial axial field strengths are increased on MagLIF experiments.

I. INTRODUCTION

Transport coefficients in advanced magnetohydrodynamics (MHD) simulations play a key role in the design and analysis of inertial confinement fusion (ICF) experiments.[1–3] Various research groups have used different modeling and fitting techniques to calculate transport coefficients as functions of magnetic field and ionization.[4–8] These transport coefficients differ from analytically derived transport coefficients in that they are provided as functional fits to the results of kinetic simulations. It is important to understand how the different transport coefficient models may impact the MHD simulations used to design and analyze high-valued ICF and high energy density physics (HEDP) experiments. To this end, we have studied the sensitivities of different transport coefficient models in an ICF concept called magnetized liner inertial fusion (MagLIF).[2,3]

MagLIF is studied experimentally on the 20–30 MA, 100 ns Z facility at Sandia National Laboratories.[9,10] In MagLIF, the Z facility implodes an initially solid-metal cylindrical shell (called a liner), usually made of beryllium or aluminum. The radially imploding cylindrical shell compresses preheated ($\sim$100 eV) and premagnetized ($\sim$10 T) fusion fuel. Near stagnation, the hot fuel region reaches temperatures of a few keV, and the magnetic field is flux compressed to $\gtrsim$ 5 kT (Ref. 11) leading to magnetized electrons and ions. Typical parameters and evolution of a MagLIF shot, taken from a semi-analytic MagLIF model (SAMM) simulation (see Sec. IV for further discussion), are shown in Fig. 1.

The fuel is comprised of either pure deuterium or deuterium–tritium mixtures. Pre-magnetization is accomplished with a separate Helmholtz coil pair[12] or an auto-magnetizing liner,[13,14] and the fuel
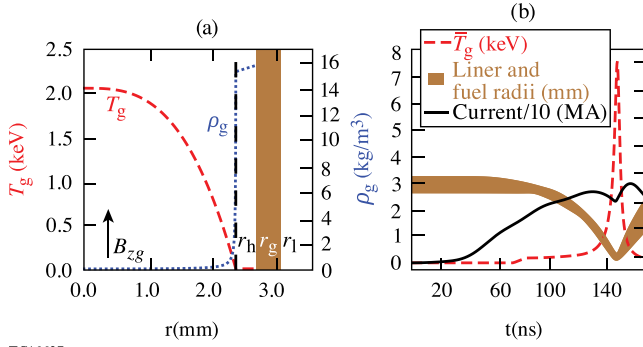
FIG. 1. (a) Diagram of the regions modeled in SAMM, including the hotspot ($0 < r < r_h$) and shelf ($r_h < r < r_g$) subregions within the gas region, and the liner ($r_g < r < r_l$) and vacuum regions ($r > r_l$). (b) Overview of a SAMM simulation of the 2010 point design[2] (modified to have smaller preheat radius $r_{ph0} = \frac{1}{4} r_{g0}$), showing the current (MA/10), liner trajectory (mm), and average gas temperature $\bar{T}_g$ (keV).

preheating is accomplished with the few-kilojoule Z beamlet laser (ZBL).[15] In addition to the Z facility, MagLIF-relevant experiments are also conducted at the OMEGA laser facility and the National Ignition Facility (NIF) in the form of scaled-down laser-driven "mini-MagLIF"[16–24] experiments and ignition-scale experiments for the study of magnetized laser preheat,[25] respectively. The MagLIF-relevant NIF shots used a range of applied axial magnetic field strengths up to 24 T, and achieved coupled laser preheat energies ranging up to 27.2 kJ.

MagLIF experiments are simulated using sophisticated multiphysics MHD codes, such as LASNEX,[3,26] HYDRA,[11] and GORGON,[27] as well as simplified codes like the semi-analytic MagLIF model (SAMM).[28,29] For the purpose of this article (i.e., quickly testing transport coefficient sensitivities over a broad parameter space), the SAMM code is particularly useful since a given MagLIF simulation can be run in approximately 30 s on a laptop. The SAMM code includes modeling of laser preheating of the fuel, pulsed-power-driven liner implosion, liner compressibility, artificial viscosity, internal magnetic pressure, ohmic heating, adiabatic compression and heating of the fuel, radiative losses and fuel opacity, magnetic flux compression with Nernst thermoelectric losses, magnetized electron and ion thermal conduction losses, end losses, enhanced losses due to prescribed dopant concentrations and contaminant mix, fusion reactions, and magnetized α-particle fuel heating.

Key physics processes in MagLIF are directly modified by the choice of transport model. Steep temperature gradients induced by the limited spatial extent of the laser preheating leads to enhanced magnetic flux losses from the fuel region to the liner via the Nernst effect, the magnitude of which is controlled by the Nernst transport coefficient.[10] Thermal conduction losses out of the hot fuel are also strongly controlled by thermal conductivity coefficients. More broadly speaking, transport effects, and thus the transport coefficients, play an important role whenever there are significant driving terms such as temperature gradients and currents, as discussed further in Sec. II.

II. THEORY OF TRANSPORT COEFFICIENTS IN EXTENDED MHD

Transport coefficients are the constants of proportionality that relate driving terms (i.e., temperature gradients and currents) to their

corresponding perturbations of the zeroth order Maxwellian distribution function. In magnetized plasmas, they govern both magnetic field and heat transport. Considering magnetic-field transport first, transport coefficients appear when Coulomb collisions are accounted for in an Ohm's law.[4] The tensor extended magnetohydrodynamic (MHD) generalized Ohm's law is given by[4,5,8]

$$\mathbf{E} = -\mathbf{u} \times \mathbf{B} + \frac{\mathbf{J} \times \mathbf{B}}{e n_e} - \frac{\nabla \cdot \underline{P}_e}{e n_e} + \frac{m_e \underline{\alpha} \cdot \mathbf{J}}{e^2 n_e \tau} - \frac{\underline{\beta} \cdot \nabla T_e}{e}. \quad (1)$$

The first term on the right-hand side of Eq. (1) gives the ideal MHD Ohm's law, dependent on the fluid velocity $\mathbf{u}$ and magnetic field $\mathbf{B}$. The second and third terms are the Hall term and electron pressure term, respectively, with the current density $\mathbf{J}$, electron pressure tensor $\underline{P}_e$, and electron density and charge, n_e and e. The second to last term in Eq. (1) includes the resistivity transport coefficient tensor $\underline{\alpha}$ and the driving current density $\mathbf{J}$, where m_e is the electron mass, and τ is the mean time between electron Coulomb collisions (the inverse of the collision frequency). Similarly, the last term includes the thermoelectric transport coefficient tensor $\underline{\beta}$ and a driving electron temperature gradient ∇T_e.

Expanding out the last two terms of Eq. (1), one can isolate each transport coefficient in a direction relative to $\mathbf{B}$ and the driving factors $\mathbf{J}$ and ∇T_e. The commonly used Braginskii formulation,[4,7] which was used by Braginskii,[4] Epperlein and Haines,[5] and Ji and Held[6] for their transport models, is given by

$$\mathbf{E} = -\mathbf{u} \times \mathbf{B} + \frac{\mathbf{J} \times \mathbf{B}}{n_e e} - \frac{\nabla \cdot \underline{P}_e}{n_e e}$$
$$+ \frac{m_e}{e^2 n_e \tau} \left[\alpha_{\parallel} \mathbf{b}(\mathbf{b} \cdot \mathbf{J}) + \alpha_{\perp} \mathbf{b} \times (\mathbf{J} \times \mathbf{b}) - \alpha_{\wedge} (\mathbf{b} \times \mathbf{J}) \right]$$
$$- \frac{\beta_{\parallel}}{e} \mathbf{b}(\mathbf{b} \cdot \nabla T_e) - \frac{\beta_{\perp}}{e} \mathbf{b} \times (\nabla T_e \times \mathbf{b}) - \frac{\beta_{\wedge}}{e} (\mathbf{b} \times \nabla T_e), \quad (2)$$

where $\mathbf{b}$ is the magnetic-field unit vector. As illustrated in Fig. 2, the directions of the transport coefficients are denoted by $\parallel$, $\perp$, and $\wedge$ subscripts, where $\parallel$ indicates the direction parallel to both the magnetic field and the driving factor, $\perp$ indicates the direction perpendicular to the magnetic field and parallel to the driving factor, and $\wedge$ indicates the direction perpendicular to both the magnetic field and driving factor. While Braginskii's formulation is physically correct, its form for the transport coefficients, particularly the perpendicular coefficients,
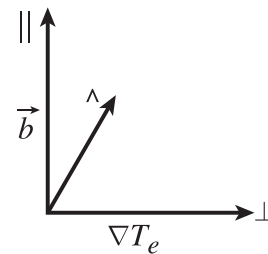
FIG. 2. Transport coefficient directions relative to the magnetic field and the driving term (∇T_e as shown here, for example). The orientation chosen here reflects the directionality of MagLIF with the magnetic field pointing vertically upward and ∇T_e pointing radially inward.

makes it more difficult to find correct fitting functions that are physical and have the correct asymptotic behavior, as discussed in Sec. III. Additionally, it does not make clear which terms are source, advection, or diffusion terms.

The disadvantages of Braginskii's formulation motivated a reformulation of the Ohm's law. Davies[7] and Sadler[8] independently arrived at a new formulation given by

$$\mathbf{E} = \frac{m_e \alpha_\parallel}{\mu_0 e^2 n_e \tau} \nabla \times \mathbf{B} - (\mathbf{u}_B \times \mathbf{B}) - \frac{\nabla \cdot \underline{P}_e}{en_e}, \quad (3)$$

with the corresponding magnetic field evolution given by

$$\frac{\partial \mathbf{B}}{\partial t} = \frac{m_e \alpha_\parallel}{\mu_0 e^2 n_e \tau} \nabla^2 \mathbf{B} + \nabla \times (\mathbf{u}_B \times \mathbf{B}) + \nabla \times \frac{\nabla \cdot \underline{P}_e}{en_e}, \quad (4)$$

where the first, second, and third terms on the right-hand side correspond to magnetic-field diffusion, advection, and the Biermann battery source term, respectively. The magnetic field advection velocity $\mathbf{u}_B$ is given by

$$\mathbf{u}_B = \mathbf{u} - (1 + \delta_\perp)\frac{\mathbf{J}}{en_e} + \delta_\wedge \frac{\mathbf{J} \times \mathbf{b}}{en_e} - \gamma_\perp \frac{\tau}{m_e} \nabla T_e + \gamma_\wedge \frac{\tau}{m_e}(\nabla T_e \times \mathbf{b}), \quad (5)$$

where $\delta_\perp = \alpha_\wedge/\chi_e$, $\delta_\wedge = (\alpha_\perp - \alpha_\parallel)/\chi_e$, $\gamma_\perp = \beta_\wedge/\chi_e$, and $\gamma_\wedge = (\beta_\parallel - \beta_\perp)/\chi_e$. The term χ_e is the electron Hall parameter, equal to $\omega_{ce}\tau$, where $\omega_{ce} = eB/m_e$ is the electron cyclotron frequency. Note that this formulation uses the difference between perpendicular and parallel coefficients rather than perpendicular coefficients by themselves, and that the direction subscripts have changed to match the directions in which the associated terms act. For example, the Nernst velocity term, with the coefficient $\gamma_\perp$, acts perpendicular to the magnetic field and parallel to the driving factor, as indicated by the $\perp$ subscript in $\gamma_\perp$.

This new Ohm's law has several advantages compared to Braginskii's formulation. First, it is more conducive to finding fitting functions without unphysical properties. The incorrect fitting functions for the perpendicular electrothermal and resistivity coefficients used by Epperlein and Haines, and Ji and Held, as discussed later, can lead to unphysical behavior in cross field magnetic-field transport (both current driven and temperature gradient driven).[7] The fits of Epperlein and Haines, and Ji and Held, therefore, can lead to incorrect modeling of magnetic-field transport, and, by extension, the overall plasma evolution.[8] In addition to the transport coefficients themselves, the terms from Braginskii's formulation have been rearranged into a more physically meaningful way in Eq. (3) by grouping them into diffusion, advection, and source terms.

In addition to magnetic-field transport, transport coefficients also affect the transport of electron and ion thermal energy. Among the models studied in this paper that account for heat transport, all of them do so in qualitatively the same way, with the same representations for the transport coefficients (unlike the magnetic field transport for which Davies and Sadler recast the parallel and perpendicular coefficients). Quantitative differences between the models do arise, however, from how the coefficients and their fits are calculated. Following Refs. 5 and 8, heat flow is described by

$$\mathbf{q}_e = -\frac{n_e T_e \tau}{m_e} \underline{\kappa} \cdot \nabla T_e - \frac{T_e}{e} \underline{\beta} \cdot \mathbf{J}, \quad (6)$$

where $\underline{\kappa}$ is the thermal conductivity transport coefficient tensor with a corresponding temperature gradient driving term.

III. CALCULATION AND FITTING OF TRANSPORT COEFFICIENTS

After identifying the transport coefficients in the magnetic transport equations [Eqs. (3) and (5)] and in the heat transport equation [Eq. (6)], two distinct steps are taken before arriving at a set of coefficients that can be used practically in an MHD simulation code. First, the transport coefficients are calculated at specific values of χ_e and ionization Z, using one of two methods: a Laguerre expansion (LE) or a direct numerical solution of the Fokker–Planck equation (FPE). Then, fits are found for these values, yielding transport coefficient functions that are continuous functions of χ_e. Fits can be made for given discrete values of Z, or can be made continuous functions of Z in addition to χ_e. Fits can be found for the ion transport coefficients in the same manner as functions of Z and $\chi_i = \omega_{ci}\tau_{ii}$, where $\omega_{ci} = ZeB/m_i$ is the ion cyclotron frequency and τ_{ii} is the ion–ion collision time. Note that in Secs. IV–V, we will be focusing on purely hydrogenic fuel ($Z = 1$) and only transport processes within the fuel (rather than liner), but we discuss the Z dependence of all the models in this section for completeness. In addition, electron and ion viscosity are important considerations, but are not considered in this paper as they are not included in SAMM.

Both of these steps—the calculating and the fitting—can introduce errors to the final set of transport coefficients. The fitting functions as well as their derivatives should be continuous, i.e., should not have discontinuities in (χ_e, Z). The calculation method and Z dependence for each transport model are summarized in Table I, as well as which of the three transport coefficients in SAMM are included in each model.

Braginskii as well as Ji and Held use an LE of the anisotropic part of the particle distribution function. Braginskii uses three terms in the expansion of f_1, the anisotropic part of the distribution function, and produces continuous fits to the transport coefficient values in χ_e and at $Z = 1, 2, 3, 4, \infty$ to an accuracy of 20%.[4,7] Note that $Z = \infty$ refers to a calculation including only electron–ion scattering, so it should be valid as $Z \to \infty$ and electron–electron collisions become negligible. The Ji–Held model uses up to 160 terms, enough terms in the Laguerre expansion such that the results varied by less than 1%. The model gave fits in χ_e and Z for $Z = 0, 1, \ldots, 100$, with each fit matching the 160 term solution to better than 1%,[6,7] although this level of

TABLE I. Summary of the transport coefficient models, including calculation method, Z dependence in the model's fits, and which of the three given transport coefficients were calculated. These three transport coefficients ($\kappa_e^\perp$, $\kappa_i^\perp$, and $\beta_\wedge$) are the ones in included in SAMM.

Model	Method	Z dependence	$\kappa_e^\perp$	$\kappa_i^\perp$	$\beta_\wedge$
Braginskii	LE, 3 terms	1,2,3,4, ∞	$\times$	$\times$	$\times$
Epperlein–Haines	FPE	1–8, 10, 12, 14, 20, 30, 60, ∞	$\times$		$\times$
Ji–Held	LE, up to 160 terms	0–100	$\times$	$\times$	$\times$
Davies	FPE	$Z \geq 1$			$\times$
Sadler	FPE	$Z \geq 1$	$\times$		$\times$

accuracy is misleading for some of the coefficients given the unphysical fitting formulas used, as will be discussed later. Note that $Z = 0$ corresponds to only electrons, so these coefficients could be used in a two-fluid code where there could be regions containing only electrons.

In contrast, Epperlein and Haines, Davies, and Sadler use a direct numerical solution of the Fokker–Planck equation. The Epperlein–Haines model uses finite differences (in velocity space) of the f_1 equation to numerically solve for the transport coefficients, and provide fits in χ_e and at $Z = 1 - 8, 10, 12, 14, 20, 30, 60$, and $Z \to \infty$, within an accuracy of 15%, again, misleading because of some of their unphysical fitting formulas. Davies and Sadler employ a similar technique but provide fits for arbitrary $Z \geq 1$.

Note that the numerical results (i.e., the calculated values of the transport coefficients before fitting) for Epperlein and Haines, Ji and Held, Davies, and Sadler are essentially equivalent. (Only the numerical results of Braginskii are different from the rest since only three terms in the LE were used, which is not enough to achieve sufficient accuracy as Ji and Held showed.) Yet, there are still significant differences between the models because of the choices for fitting functions. In particular, the Epperlein–Haines and Ji–Held fits for the perpendicular electrothermal and resistivity coefficients are fundamentally unphysical because of their incorrect limiting behavior. Both the coefficient values themselves, as well as their derivatives with respect to χ_e, should be zero at $\chi_e = 0$, such that there is no cross field transport when **B** = 0. The derivatives should be zero at $\chi_e = 0$ because in the induction and electron internal energy evolution equations, gradients are taken of the terms with these cross field coefficients, and these terms must not contribute when **B** = 0 in order to be physically correct. The Epperlein–Haines and Ji–Held fits for the perpendicular electrothermal and resistivity coefficients do not satisfy both of these requirements. This contrasts with Braginskii, who chose to fit to a function of χ_e^2, ensuring that the derivative of the transport coefficient with respect to χ_e goes to zero as χ_e goes to zero. Davies and Sadler also use fitting functions that satisfy these requirements. This is illustrated in Fig. 3 for the perpendicular coefficients, $\alpha_\perp$, $\beta_\perp$, $\kappa_e^\perp$, and $\kappa_i^\perp$.

In addition to the errors introduced by calculating and fitting to the transport coefficients, there are also assumptions made by the transport models that limit their general applicability. There are the assumptions of linear transport theory common to all the transport models. The anisotropic part of the distribution function should be

much smaller than the (isotropic) Maxwellian part, and temperature and density gradients should be shallow: $v_{th}\tau|\nabla T_e|/T_e \ll 1$ and $v_{th}\tau|\nabla n_e|/n_e \ll 1$, where v_{th} is the thermal velocity. There are also assumptions relating to the initial conditions of the simulations used by Epperlein–Haines, Davies, and Sadler. For example, Sadler assumed a fixed electric field and varied the transverse magnetic field, while Davies used a constant externally applied magnetic field.

To summarize, while all five transport models stem from the same physics of extended MHD, different choices are made in the calculation and fitting methods, some of which significantly impact the final transport coefficients. All five transport models use physically equivalent Ohm's laws, despite their different forms. Furthermore, except for Braginskii, their numerical results from calculating the transport coefficients are all essentially equal. However, Epperlein–Haines and Ji–Held use fitting formulas that give unphysical values for the perpendicular electrothermal and resistivity coefficients at $\chi_e \ll 1$, unlike Braginskii, Davies, and Sadler whose fitting functions do give the correct limiting behavior. In addition to the limiting values, the transport coefficients also vary between each model at intermediate values of χ_e and χ_i as a result of the fitting formulas. Some of these differences are illustrated in Fig. 4, which shows how the fitting functions from each model for several transport coefficients vary as a function of χ_e relative to Braginskii's fit values.

The comparison was made to Braginskii in Fig. 4 because he provided the first set of transport coefficients and they have a long history of usage in MHD simulations. The rest of this paper presents results from simulations designed to uncover and explain differences between the transport models.

Before proceeding, we note that not all transport coefficients are provided by every model. For example, ion coefficients are often omitted altogether (largely due to the difficulty of adapting Fokker–Planck simulations from electrons to ions). Thus it is sometimes necessary to combine different models in order to account for all transport effects in SAMM. See Table I for which coefficients in SAMM are included in each transport model.

IV. TRANSPORT COEFFICIENTS AND DEPENDENCIES IN SAMM

SAMM is a 1D, semi-analytic code for modeling magnetized liner inertial fusion (MagLIF).[28] It consists of a central fuel region (i.e., a gas
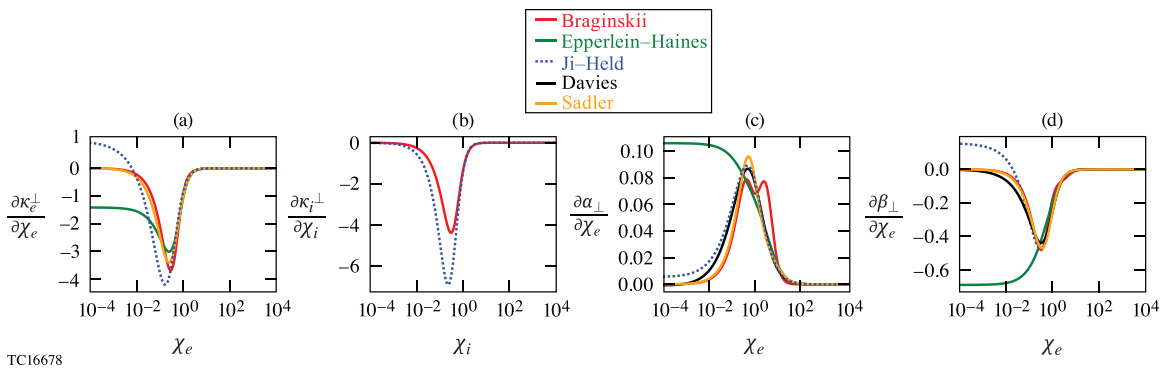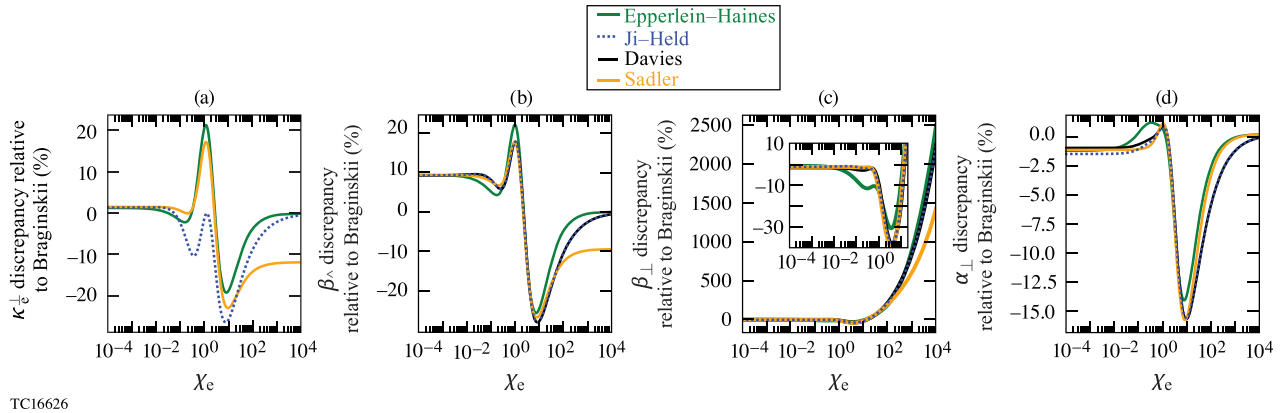
FIG. 3. Derivatives of perpendicular thermal conductivity coefficients, $\kappa_e^\perp$ and $\kappa_i^\perp$, and perpendicular resistivity and electrothermal coefficients, $\alpha_\perp$ and $\beta_\perp$, with respect to the electron or ion Hall parameter, χ_e or χ_i, respectively: (a) $\partial\kappa_e^\perp/\partial\chi_e$. (b) $\partial\kappa_i^\perp/\partial\chi_i$. (c) $\partial\alpha_\perp/\partial\chi_e$. (d) $\partial\beta_\perp/\partial\chi_e$. $Z = 1$ is used here. Note that ion transport coefficients are only provided by Braginskii and Ji–Held.

FIG. 4. Discrepancies, relative to Braginskii and as a function of the Hall parameter $\chi_e = \omega_{ce}\tau$, of each model's electron transport coefficients in SAMM. (a) Perpendicular electron thermal conductivity coefficient $\kappa_e^\perp$. (b) Cross-field electrothermal (i.e., Nernst) coefficient $\beta_\wedge$, as well as the perpendicular coefficients corrected by Refs. 7 and 8. (c) Perpendicular electrothermal (i.e., cross field Nernst) $\beta_\perp$. (d) Perpendicular resistivity coefficient, $\alpha_\perp$. $Z = 1$ is used here. Note the log scale and that thermal conductivity coefficients, such as $\kappa_e^\perp$, are not provided by Davies.

region), a liner region, and an outer vacuum region and it can model the 1D evolution of the liner trajectory and fuel region properties like temperature profiles, as shown in Fig. 1.

As is often done in MHD codes, the transport coefficients are calculated in SAMM from rational polynomial fits, which are provided by the transport model being used and found in the manner discussed in Sec. I. Note that in the following analysis, we ignore contaminant mix, assuming purely hydrogenic fuel ($Z = 1$), thus suppressing the Z dependence in the transport coefficient fits. In addition, magnetic diffusion is not modeled in SAMM because in a MagLIF experiment with a hot gas region, Nernst flux losses dominate the flux losses caused by magnetic diffusion,[28] so the perpendicular resistivity coefficient is not included in the following analysis. Finally, since spatial variations in SAMM are only allowed in the radial direction, only the perpendicular and cross coefficients are relevant here. These conditions yield the following three coefficients which we model: $\kappa_e^\perp = \kappa_e^\perp(\chi_e)$, $\kappa_i^\perp = \kappa_i^\perp(\chi_i)$, and $\beta_\wedge = \beta_\wedge(\chi_e)$.

In SAMM, these transport coefficients directly modify the electron and ion thermal conduction losses, P_{ce} and P_{ci}, and the magnetic flux losses from the gas region into the liner, $\dot{\Phi}_{zg}$, as follows:

$$P_{ce}(r) = 2\pi r h \cdot \kappa_e^\perp(\chi_e) \cdot k_B \frac{\partial T_g}{\partial r}, \tag{7}$$

$$P_{ci}(r) = 2\pi r h \cdot \kappa_i^\perp(\chi_i) \cdot k_B \frac{\partial T_g}{\partial r}, \tag{8}$$

$$\dot{\Phi}_{zg} = \left[-2\pi r h \cdot \beta_\wedge(\chi_e) \cdot \frac{k_B}{q_e} \frac{\partial T_g}{\partial r} \right]_{r = r_g}, \tag{9}$$

where $r_g = r_g(t)$ is the radius of gas–liner interface, and h is the height of the liner.

To provide a sense of the values of the transport coefficients themselves within the regions of the imploding fuel (namely, the less-dense hotspot region, and the denser cold-shelf region), we plot as a function of time in Fig. 5 illustrative values of the transport coefficients, $\kappa_e^\perp$, where the bar denotes volume averaging, and $\beta_\wedge(r = r_g)$, the Nernst coefficient at $r = r_g$. These were taken from a simulation of the 2010 point design,[2] modified to have a preheat radius less than the gas radius,
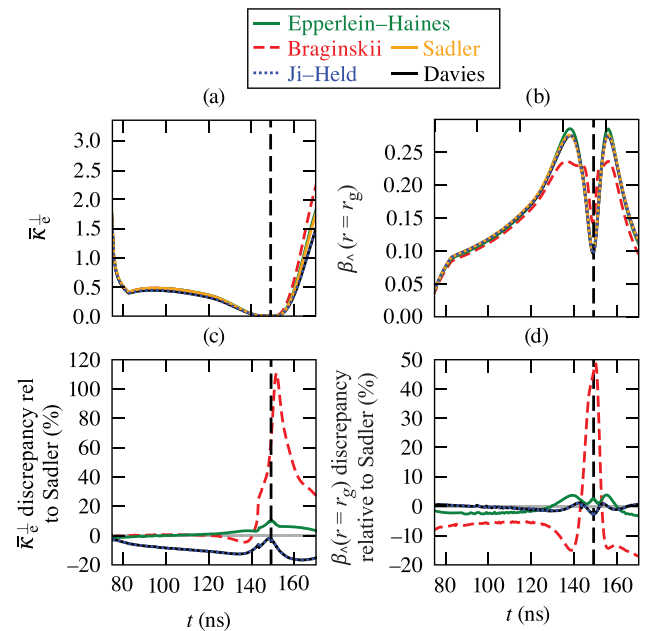
FIG. 5. (a) Volume averaged electron thermal conduction coefficient $\bar{\kappa}_e^\perp$. (b) Nernst coefficient at $r = r_g$, $\beta_\wedge(r = r_g)$. The discrepancy of (a) and (b), given as a percent discrepancy relative to Sadler, is shown in (c) and (d), respectively. These curves were taken from SAMM simulations of the same design as in Fig. 1(b). The time axis starts at the laser preheat start time. The bang time for the Sadler run is indicated by the vertical dashed line at $t \approx 149$ ns. Note that the Davies curve lies on top of the Ji–Held curve.

$r_{ph0} = \frac{1}{4} r_{g0}$. Figures 5(a) and 5(b) show the coefficient values themselves, while Figs. 5(c) and 5(d) shows these values relative to Sadler.

V. RESULTS

To test the cumulative impact of different modeling choices one makes when selecting a set of transport coefficients, we compare the

coefficients' integrated effect on various values of interest like the fusion yield. We also look at the transport coefficients' effect on the burn- and volume-averaged fuel temperature, $\langle \bar{T}_g \rangle$, and the percent of magnetic flux, f_Φ, that has been lost at the time of peak burn t_{bang}, defined as follows:

$$\langle \bar{T}_g \rangle \equiv \frac{\int_0^{t_{end}} \bar{T}_g(r)\dot{N}(t)\mathrm{d}t}{\int_0^{t_{end}} \dot{N}(t)\mathrm{d}t}, \tag{10}$$

where

$$\bar{T}_g(t) \equiv \frac{\int_0^{r_g(t)} T_g(r,t) \cdot 2\pi rh\mathrm{d}r}{\int_0^{r_g(t)} 2\pi rh\mathrm{d}r} \tag{11}$$

and

$$f_\Phi \equiv \left[1 - \frac{\Phi_{zg}(t=t_{bang})}{\Phi_{zg}(t=0)} \right] \times 100, \tag{12}$$

where $\dot{N} = \dot{N}(t)$ is the neutron production rate and t_{end} is the simulation end time when $\dot{N} \approx 0$. These quantities were selected because they are more directly impacted by the choice of transport coefficients.

Parameter scans across the laser preheat energy, E_{ph}, from 500 J to 20 kJ, and the initial axial magnetic field, B_{z0}, from 0 to 50 T sample a large region of parameter space for each transport model. These two parameters, E_{ph} and B_{z0}, are both particularly important in determining the plasma transport properties, as they affect the total energy deposited in the fuel and the degree of confinement, respectively. The different B_{z0} values lead to different levels of magnetization, χ_e, which is an argument for all the transport model fits, and thus has a direct impact on the transport properties. Similarly, different E_{ph} values lead to different hotspot energies and, by extension, different temperature gradients ∇T_e, which will influence magnetic field transport as the magnetic-field is advected down the temperature gradient in proportion to ∇T_e via the Nernst term.

As mentioned in Sec. IV, not every transport coefficient is included in each model, requiring some combination of the different models. For the sake of a clearer comparison and its long-standing and frequent usage, we use Braginskii's ion thermal conduction coefficient $\kappa_i^\perp$ for all models (including Ji and Held's), allowing us to compare only the electron (thermal conduction and Nernst) coefficients in SAMM, $\kappa_e^\perp$ and $\beta_\wedge$, between the five models. At $\chi_e \approx 7$, perpendicular thermal conductivity becomes lower for electrons than ions, though, so a comparison between the ion thermal conductivity coefficients (provided namely, by Braginskii and Ji and Held) is also of interest for MagLIF. Additionally, note that out of the transport coefficients included in SAMM, Davies only provides a new fit for the Nernst velocity coefficient, $\beta_\wedge$, so we test Davies' Nernst velocity coefficient along with Ji–Held's electron thermal conduction coefficient since Davies' coefficients were derived as modifications and extensions to Ji and Held's fits.

For all the SAMM simulations in the parameter scans, we used a slightly modified version of the 2010 point design,[2] setting the initial preheat radius to a quarter of the gas radius, rather than the gas radius

so as to produce both a central "hotspot" and outer "cold-shelf" region within the fuel.

To begin, we look at the discrepancies between the models, relative to Sadler, of the burn- and volume-averaged electron thermal conduction coefficient, $\langle \bar{\kappa}_e^\perp \rangle$, and burn-averaged Nernst coefficient at $r = r_g$, $\langle \beta_\wedge(r = r_g) \rangle$. The bar and angle brackets denote volume and burn averaging, respectively [see Eqs. (10) and (11)]. Except for the magnetic flux losses, f_ϕ, the discrepancy is represented as a percent difference of the given model's value relative to Sadler's value for each SAMM simulation at a given point in the (E_{ph}, B_{z0}) parameter space. For example, for $\langle \bar{T}_g \rangle$, the discrepancy is represented as $\Delta \langle \bar{T}_g \rangle [\%] = 100 \times (\langle \bar{T}_g \rangle_M / \langle \bar{T}_g \rangle_S - 1)$, where the M and S subscripts correspond to the given model and Sadler, respectively. For the flux losses, the discrepancy is instead represented as a ratio $\Delta f_\phi = f_{\phi,M}/f_{\phi,S}$. Discrepancies relative to Sadler are presented instead of discrepancies relative to Braginskii because most of the averaged values (such as $\langle \bar{T}_g \rangle$) that were found using Braginskii vary substantially from the rest of the models which have relatively closer values. Thus comparing to Braginskii would obscure, in Figs. 6–8, the more subtle differences between the rest of models. As shown in Fig. 6, in many regions of the (E_{ph}, B_{z0}) parameter space, $\langle \bar{\kappa}_e^\perp \rangle$ and $\langle \beta_\wedge(r = r_g) \rangle$ vary significantly, up to ~73% and ~46%, respectively. The Braginskii values generally have the largest discrepancies relative to Sadler, throughout most of the parameter space, while the other models, including Epperlein–Haines, Ji–Held, and Davies, vary less than ~10% relative to Sadler. This indicates the importance of the specific fit function values at intermediate χ_e, in addition to the correct limiting behavior.

As shown in Eqs. (7)–(9), the transport coefficients have a direct impact on the electron and ion thermal conduction losses and magnetic-flux losses, respectively. To assess this impact, we consider $\langle \bar{T}_g \rangle$ and f_Φ across the (E_{ph}, B_{z0}) space. In the $\langle \bar{T}_g \rangle$ plots shown in Figs. 7(a)–7(e), we see correlations with the transport coefficient figures as expected. That is, regions of lower $\langle \bar{\kappa}_e^\perp \rangle$ and $\langle \beta_\wedge(r = r_g) \rangle$ (relative to Sadler) generally exhibit higher $\langle \bar{T}_g \rangle$. The magnetic flux loss discrepancies, shown in Figs. 7(f)–7(j), exhibit a qualitatively different structure in (E_{ph}, B_{z0}) space compared to the $\langle \bar{T}_g \rangle$ results. Sensitivity of f_Φ is much larger to the choice of transport coefficients between Sadler and Braginskii around the border in (E_{ph}, B_{z0}) space between negligible f_Φ and significant f_Φ [see Figs. 7(f) and 7(g)], giving discrepancies of a factor of ~3 in f_Φ. This sensitivity is less pronounced for the three other models.

We also compare the fusion yield discrepancies between the various models relative to Sadler in Fig. 7. Figure 7(k) shows the fusion yield in (E_{ph}, B_{z0}) space for the Sadler coefficients, highlighting the region in (E_{ph}, B_{z0}) space with the optimal yield at $E_{ph} \simeq 5$ kJ and $B_{z0} \simeq 40$ T. Figures 7(l)–7(o) shows the discrepancies between the given model and Sadler, illustrating the integrated outcome of a model's transport coefficients on the fusion yield, with discrepancies up to ~38%. Qualitatively and quantitatively similar patterns in the fusion yield discrepancies are seen across the four models relative to Sadler. There is close to zero discrepancy in the region of optimal yield, while in other regions, yield discrepancies can be significantly higher or lower. Despite the similarity of the fits between Davies and Sadler, there are significant differences in the fusion yield, up to ~ 38%, at low B_{z0}, again illustrating the importance of the transport coefficient fit values themselves, besides just the form and correct limiting behavior. Such discrepancies could be resolved with experiments targeting
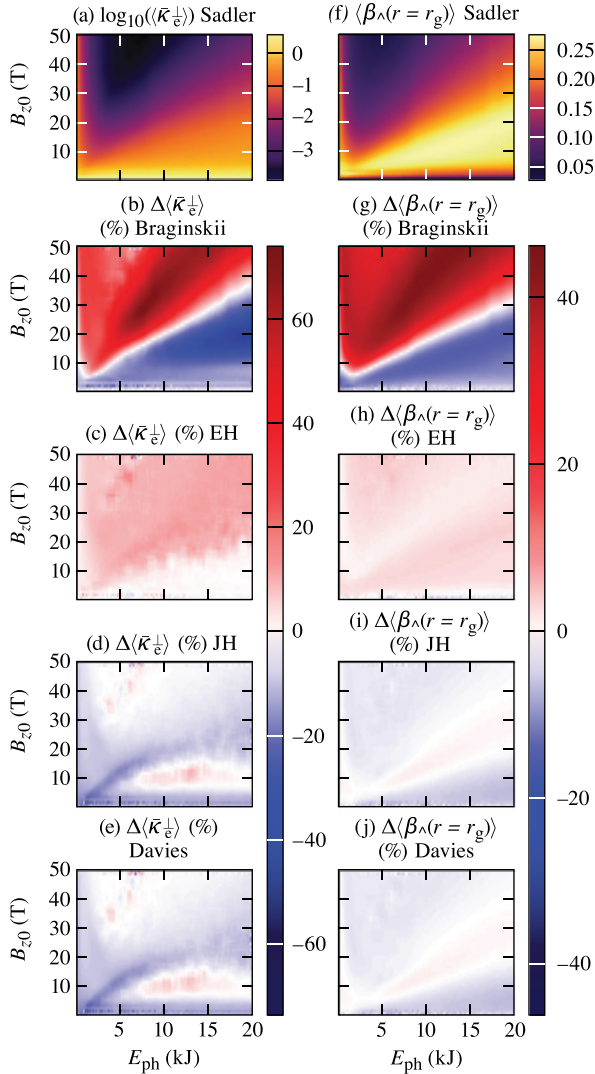
TC16701J1

FIG. 6. Summary of transport coefficient discrepancies between each model and Sadler across the (E_{ph}, B_{z0}) parameter space: (a) $\langle \bar{\kappa}_e^\perp \rangle$. (b) $\langle \beta_\wedge (r = r_g) \rangle$. (c)–(j) are percentage discrepancies (%) between each model and Sadler.

specific points in (E_{ph0}, B_{z0}) space to determine which transport coefficient models are more accurate.

In Figs. 6 and 7, following from the discrepancies for each model relative to Sadler in the transport coefficient values, to the $\langle \bar{T}_g \rangle$ and f_Φ values, and finally to the yields, we see how lower (higher) transport coefficients lead to higher (lower) averaged temperatures and less (more) magnetic-flux losses, finally resulting in higher (lower) fusion yields. This provides a coherent picture of how discrepancies in the transport coefficients lead to measurable differences in a highly integrated and important value like the fusion yield.

For a more-direct evaluation of the transport coefficients' effect on the fusion yield, we divide the ratio of the fusion yield for a given model (Y_M) to the yield from Sadler (Y_S), $R_Y \equiv Y_M / Y_S$, by the ratio of the averaged transport coefficient for a given model [$\langle \bar{\kappa}_e^\perp \rangle_M$ or $\langle \beta_\wedge (r = r_g) \rangle_M$] to Sadler's averaged transport coefficient [$\langle \bar{\kappa}_e^\perp \rangle_S$ or $\langle \beta_\wedge (r = r_g) \rangle_S$]: $R_\kappa \equiv \langle \bar{\kappa}_e^\perp \rangle_M / \langle \bar{\kappa}_e^\perp \rangle_S$ or $R_\beta \equiv \langle \beta_\wedge (r = r_g) \rangle_M / \langle \beta_\wedge (r = r_g) \rangle_S$. That is, we plot R_Y / R_κ and R_Y / R_β across (E_{ph}, B_{z0}) space, as shown in Fig. 8. This allows us to more-directly assess the effect of transport coefficient discrepancies on an integrated, observable value like the yield (and how that effect varies based on E_{ph} and B_{z0}). For example, if the (averaged) transport coefficient discrepancy is some factor (say, 1.5×), then how does that discrepancy translate into discrepancies of the fusion yield? It is shown that a given discrepancy in a transport coefficient can have a magnified or a reduced effect on the fusion yield (relative to Sadler), illustrating that the integrated effect (chosen here to be indicated by the fusion yield) of the choice of transport coefficients depends on the region of (E_{ph}, B_{z0}) space.

For a more-focused comparison between the transport models at just one point in (E_{ph}, B_{z0}) space, we also consider a recent high-performing MagLIF shot, Z3289, described in Ref. 10, for which $E_{ph} = 1.2\,\text{kJ}$ and $B_{z0} = 15.9\,\text{T}$. This shot had a burn-weighted average ion temperature of $3.1\,\text{keV}$ and a yield of 1.1×10^{13} DD neutrons. Because of the large backscatter and absorption losses from the laser propagating through the laser entrance hole (LEH) window, the pre-heat energy coupled to the fuel is significantly less than the pre-LEH laser energy.[11,22,30] In the following SAMM simulations of experimental shots, we tune the coupled laser preheat energy, E_{ph}, such that the simulated primary neutron yield matches the experimental value. Simulating Z3289 with a scaled preheat energy $E_{ph} \sim 450\,\text{J}$ as just described, for the averaged transport coefficients [i.e., $\langle \bar{\kappa}_e^\perp \rangle$ and $\langle \beta_\wedge (r = r_g) \rangle$], substantial discrepancies (>30%) are found between Sadler and Braginskii. However, these transport coefficient discrepancies do not translate into significant discrepancies in the flux losses and experimental observables like the averaged gas temperature and fusion yield, for any of the models, with discrepancies ≲2%. The other models have small percent discrepancies (≲5%) for both the averaged transport coefficients and f_ϕ, $\langle \bar{T}_g \rangle$, and fusion yield. Artificially scaling up the laser preheat energy by more than a factor of ∼2×, only leads to marginally higher discrepancies. Another high-performing shot, Z2591,[31] was also analyzed in this manner (a scaled preheat energy of $E_{ph} \sim 200\,\text{J}$ was found and used), and the same trend is observed. These results illustrate how coupled preheat energies on high performing MagLIF experiments thus far are too low to drive the larger temperature gradients expected to produce larger discrepancies between the transport coefficient models. Note, however, that these experiments used lower peak currents (∼20 MA) than the 2010 point design as studied in Secs. I, IV, and V, and so are in a different regime than shown, for example, in Fig. 7, and these simulation results are not directly comparable to those results with the 2010 point design.

VI. CONCLUSIONS

In this article, we have analyzed the discrepancies between five different sets of extended MHD transport coefficients using a semi-analytic code for MagLIF. There are substantial qualitative differences between some of the coefficients, namely, the perpendicular electro-thermal and resistivity coefficients found by Epperlein and Haines and Ji and Held, as a result of unphysical limiting behavior in the fitting functions, and there are also differences in all the transport coefficients simply due to different forms of fitting functions, leading to numerical
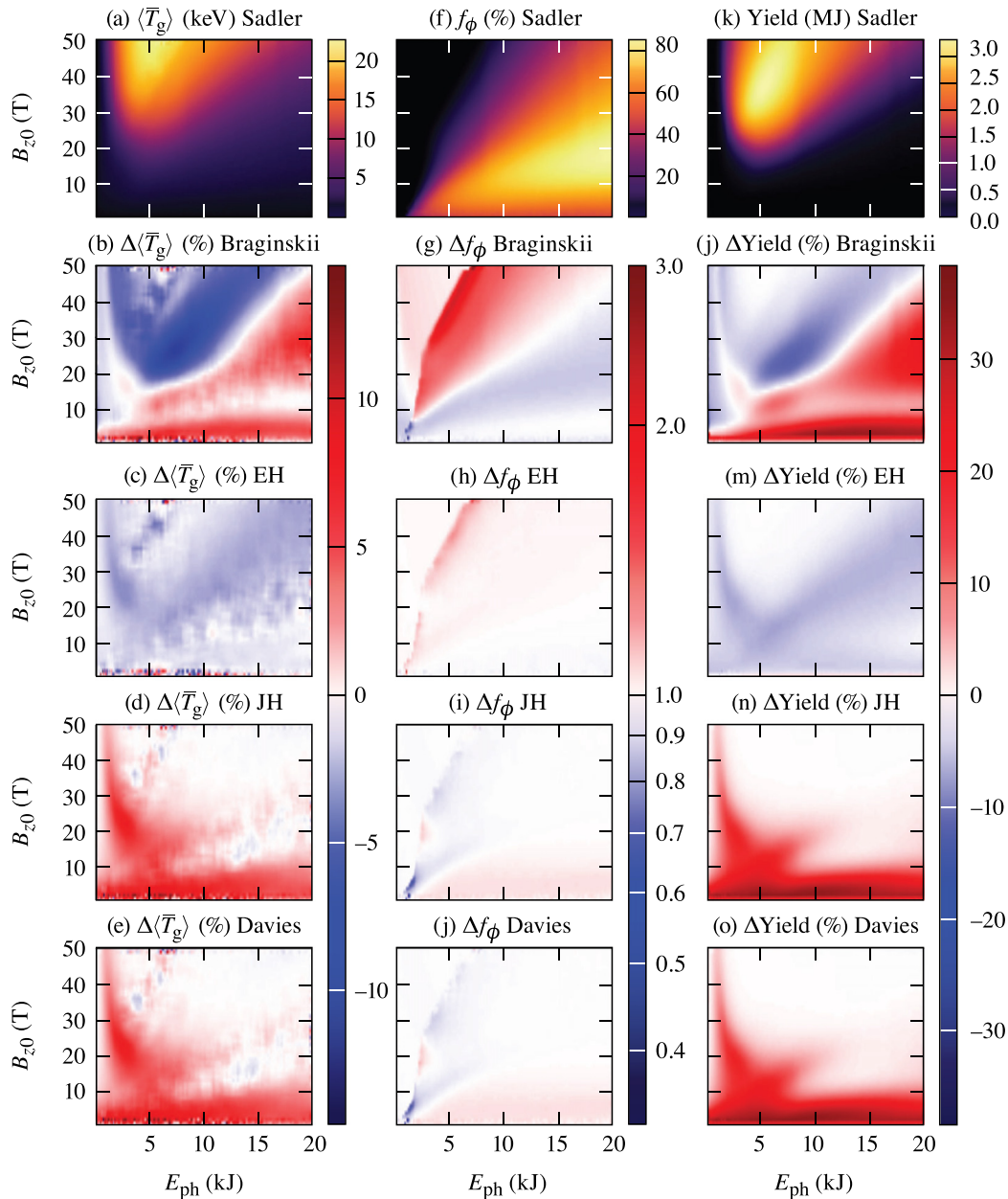
TC16702J1

FIG. 7. Summary of discrepancies in time integrated quantities between each model and Sadler across the (E_{ph}, B_{z0}) parameter space as result of the transport coefficient discrepancies: (a) burn- and volume-averaged gas temperature, (b) magnetic-flux losses, and (c) fusion yield. (d)–(o) are percentage discrepancies (%) between each model and Sadler. However, note that (e), (h), (k), and (n) are ratios relative to Sadler (b) and not percentages.

discrepancies in the simulated observables. The latter kind of discrepancy has been explored using extensive parameter scans in the (E_{ph}, B_{z0}) space, which show significant differences of up to 38% in integrated values like the fusion yield, depending on the region of (E_{ph}, B_{z0}) parameter space, with discrepancies of up to 73% between the (averaged) coefficients themselves. Given the unphysical limiting behavior of the perpendicular transport coefficients

of Epperlein–Haines and Ji–Held, and extensive kinetic simulation results of Davies and Sadler, these latest two transport coefficient models are expected to be the most accurate. However further experimental validation is needed. These results highlight the need for reassessment of past results and continued consideration of the choice of transport coefficients in extended MHD simulations.
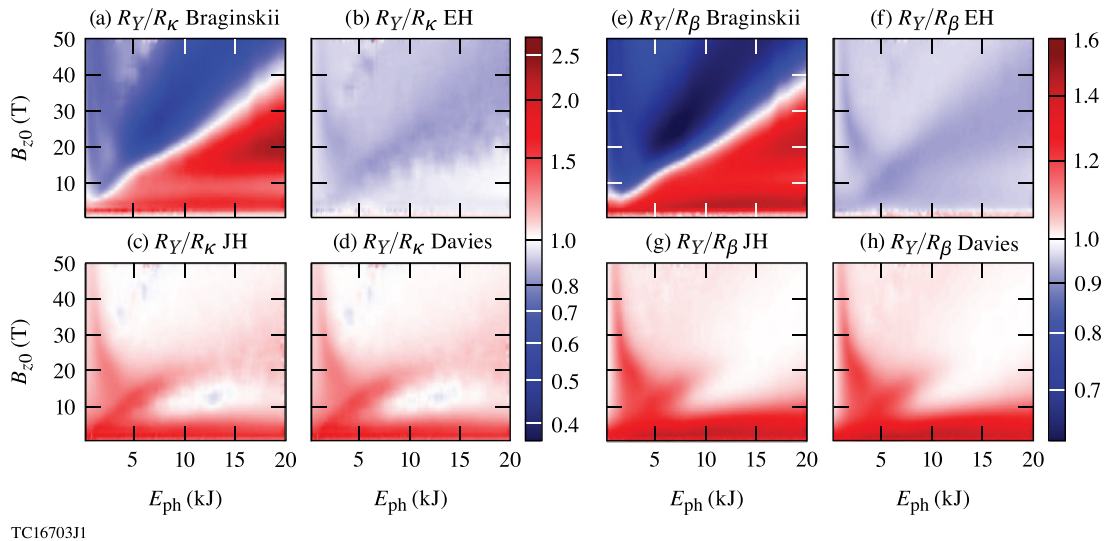
FIG. 8. Ratios, of other models relative to Sadler, of fusion yield discrepancies to $\langle \bar{\kappa}_e^\perp \rangle$ discrepancies, R_Y/R_κ: (a) Braginskii, (b) Epperlein–Haines, (c) Ji–Held, and (d) Davies. Ratios (of other models relative to Braginskii) of fusion yield discrepancies to $\langle \beta_\wedge (r = r_g) \rangle$ discrepancies, R_Y/R_β: (e) Braginskii, (f) Epperlein–Haines, (g) Ji–Held, and (h) Davies.

MagLIF is being studied in scaled-down laser-driven configurations[16–24] at the OMEGA laser facility and in ignition-scale experiments at the NIF for detailed physics studies of magnetized laser preheat.[25] Magnetized gas pipe shots on NIF have been conducted at magnetic field strengths of 0–24 T and laser preheat energies of 15.2–27.2 kJ. However, the targets utilized hydrocarbon gases mixed with spectroscopic dopants for diagnostic reasons, with future DD and DT shots being planned. These platforms could serve as testbeds for experimentally validating the transport coefficient models. In addition, increases to the laser preheat energy and initial axial field strength on the Z machine may be implemented, which would enable access to a larger region of the (E_{ph}, B_{z0}) parameter space for which to experimentally assess the transport coefficient models. The results of this article indicate where in (E_{ph}, B_{z0}) space transport coefficient models are discrepant, and thus may serve as a guide for experimental validation of the models. Such experimental validation will in turn improve the predictive capability of MHD simulation codes for MagLIF experiments and beyond.

ACKNOWLEDGMENTS

AUTHOR DECLARATIONS
Conflict of Interest

The authors have no conflicts to disclose.

Author Contributions

Y. Lawrence: Conceptualization (equal); Data curation (lead); Formal analysis (lead); Software (lead); Validation (lead); Visualization (lead); Writing – original draft (lead); Writing – review & editing (equal). **J. R. Davies:** Conceptualization (supporting); Formal analysis (supporting); Validation (equal); Writing – review & editing (equal). **R. D. McBride:** Conceptualization (supporting); Formal analysis (supporting); Software (supporting); Validation (equal); Writing – review & editing (equal). **A. B. Sefkow:** Conceptualization (lead); Formal analysis (equal); Project administration (lead); Resources (lead); Software (supporting); Validation (equal); Writing – original draft (equal); Writing – review & editing (lead).

DATA AVAILABILITY

The data that support the findings of this study are available from the corresponding author upon reasonable request.

REFERENCES

[1]E. I. Moses, J. Atherton, L. Lagin, D. Larson, C. Keane, B. MacGowan, R. Patterson, M. Spaeth, B. Van Wonterghem, P. Wegner, and R. Kauffman, J. Phys.: Conf. Ser. **688**, 012073 (2016).

[2] S. A. Slutz, M. C. Herrmann, R. A. Vesey, A. B. Sefkow, D. B. Sinars, D. C. Rovang, K. J. Peterson, and M. E. Cuneo, Phys. Plasmas **17**, 056303 (2010).

[3] S. A. Slutz and R. A. Vesey, Phys. Rev. Lett. **108**, 025003 (2012).

[4] S. I. Braginskii, in *Reviews of Plasma Physics*, edited by M. A. Leontovich (Consultants Bureau, New York, 1965), Vol. 1, p. 205.

[5] E. M. Epperlein and M. G. Haines, Phys. Fluids **29**, 1029 (1986).

[6] J.-Y. Ji and E. D. Held, Phys. Plasmas **20**, 042114 (2013).

[7] J. R. Davies, H. Wen, J.-Y. Ji, and E. D. Held, Phys. Plasmas **28**, 012305 (2021).

[8] J. D. Sadler, C. A. Walsh, and H. Li, Phys. Rev. Lett. **126**, 075001 (2021).

[9] M. R. Gomez, S. A. Slutz, A. B. Sefkow, D. B. Sinars, K. D. Hahn, S. B. Hansen, E. C. Harding, P. F. Knapp, P. F. Schmit, C. A. Jennings, and T. J. Awe, Phys. Rev. Lett. **113**, 155003 (2014).

[10] M. R. Gomez, S. A. Slutz, C. A. Jennings, D. J. Ampleford, M. R. Weis, C. E. Myers, D. A. Yager-Elorriaga, K. D. Hahn, S. B. Hansen, E. C. Harding, A. J. Harvey-Thompson, D. C. Lamppa, M. Mangan, P. F. Knapp, T. J. Awe, G. A. Chandler, G. W. Cooper, J. R. Fein, M. Geissel, M. E. Glinsky, W. E. Lewis, C. L. Ruiz, D. E. Ruiz, M. E. Savage, P. F. Schmit, I. C. Smith, J. D. Styron, J. L. Porter, B. Jones, T. R. Mattsson, K. J. Peterson, G. A. Rochau, and D. B. Sinars, Phys. Rev. Lett. **125**, 155002 (2020).

[11] A. B. Sefkow, S. A. Slutz, J. M. Koning, M. M. Marinak, K. J. Peterson, D. B. Sinars, and R. A. Vesey, Phys. Plasmas **21**, 072711 (2014).

[12] D. C. Rovang, D. C. Lamppa, M. E. Cuneo, A. C. Owen, J. McKenney, D. W. Johnson, S. Radovich, R. J. Kaye, R. D. McBride, C. S. Alexander, T. J. Awe, S. A. Slutz, A. B. Sefkow, T. A. Haill, P. A. Jones, J. W. Argo, D. G. Dalton, G. K. Robertson, E. M. Waisman, D. B. Sinars, J. Meissner, M. Milhous, D. N. Nguyen, and C. H. Mielke, Rev. Sci. Instrum. **85**, 124701 (2014).

[13] S. A. Slutz, C. A. Jennings, T. J. Awe, G. A. Shipley, B. T. Hutsel, and D. C. Lamppa, Phys. Plasmas **24**, 012704 (2017).

[14] G. A. Shipley, T. J. Awe, B. T. Hutsel, J. B. Greenly, C. A. Jennings, and S. A. Slutz, Phys. Plasmas **26**, 052705 (2019).

[15] P. K. Rambo, I. C. Smith, J. L. Porter, M. J. Hurst, C. S. Speas, R. G. Adams, A. J. Garcia, E. Dawson, B. D. Thurston, C. Wakefield, J. W. Kellogg, M. J. Slattery, H. C. Ives, R. S. Broyles, J. A. Caird, A. C. Erlandson, J. E. Murray, W. C. Behrendt, N. D. Neilsen, and J. M. Narduzzi, Appl. Opt. **44**, 2421 (2005).

[16] J. R. Davies, D. H. Barnak, R. Betti, E. M. Campbell, P. Y. Chang, A. B. Sefkow, K. J. Peterson, D. B. Sinars, and M. R. Weis, Phys. Plasmas **24**, 062701 (2017).

[17] D. H. Barnak, J. R. Davies, R. Betti, M. J. Bonino, E. M. Campbell, V. Yu. Glebov, D. R. Harding, J. P. Knauer, S. P. Regan, A. B. Sefkow, A. J. Harvey-Thompson, K. J. Peterson, D. B. Sinars, S. A. Slutz, M. R. Weis, and P.-Y. Chang, Phys. Plasmas **24**, 056310 (2017).

[18] E. C. Hansen, D. H. Barnak, P.-Y. Chang, R. Betti, E. M. Campbell, J. R. Davies, J. P. Knauer, J. L. Peebles, S. P. Regan, and A. B. Sefkow, Phys. Plasmas **25**, 122701 (2018).

[19] E. C. Hansen, D. H. Barnak, R. Betti, E. M. Campbell, P. Y. Chang, J. R. Davies, V. Y. Glebov, J. P. Knauer, J. Peebles, S. P. Regan, and A. B. Sefkow, Plasma Phys. Controlled Fusion **60**(5), 054014 (2018).

[20] J. R. Davies, R. E. Bahr, D. H. Barnak, R. Betti, M. J. Bonino, E. M. Campbell, E. C. Hansen, D. R. Harding, J. L. Peebles, A. B. Sefkow, W. Seka, P.-Y. Chang, M. Geissel, and A. J. Harvey-Thompson, Phys. Plasmas **25**, 062704 (2018).

[21] J. R. Davies, D. H. Barnak, R. Betti, E. M. Campbell, V. Yu. Glebov, E. C. Hansen, J. P. Knauer, J. L. Peebles, and A. B. Sefkow, Phys. Plasmas **26**, 022706 (2019).

[22] A. J. Harvey-Thompson, M. R. Weis, D. E. Ruiz, M. S. Wei, A. B. Sefkow, T. Nagayama, E. M. Campbell, J. A. Fooks, M. E. Glinsky, and K. J. Peterson, Phys. Plasmas **27**, 113301 (2020).

[23] E. C. Hansen, J. R. Davies, D. H. Barnak, R. Betti, E. M. Campbell, V. Y. Glebov, J. P. Knauer, L. S. Leal, J. L. Peebles, A. B. Sefkow, and K. M. Woo, Phys. Plasmas **27**, 062703 (2020).

[24] L. S. Leal, A. V. Maximov, E. C. Hansen, J. R. Davies, D. H. Barnak, J. L. Peebles, K. M. Woo, P. V. Heuer, A. B. Sefkow, and R. Betti, Phys. Plasmas **29**, 042703 (2022).

[25] B. B. Pollock, C. Goyon, A. B. Sefkow, M. E. Glinsky, K. J. Peterson, M. R. Weis, E. G. Carroll, J. Fry, A. J. Harvey-Thompson, S. B. Hansen, K. Beckwith, D. J. Ampleford, E. R. Tubman, D. J. Strozzi, J. S. Ross, and J. D. Moody, Phys. Plasmas **30**, 022711 (2023).

[26] G. B. Zimmerman and W. L. Kruer, Comments Plasma Phys. Controlled Fusion **2**, 51 (1975).

[27] J. P. Chittenden, S. V. Lebedev, C. A. Jennings, S. N. Bland, and A. Ciardi, Plasma Phys. Controlled Fusion **46**, B457 (2004).

[28] R. D. McBride and S. A. Slutz, Phys. Plasmas **22**, 052708 (2015).

[29] R. D. McBride, S. A. Slutz, R. A. Vesey, M. R. Gomez, A. B. Sefkow, S. B. Hansen, P. F. Knapp, P. F. Schmit, M. Geissel, A. J. Harvey-Thompson, C. A. Jennings, E. C. Harding, T. J. Awe, D. C. Rovang, K. D. Hahn, M. R. Martin, K. R. Cochrane, K. J. Peterson, G. A. Rochau, J. L. Porter, W. A. Stygar, E. M. Campbell, C. W. Nakhleh, M. C. Herrmann, M. E. Cuneo, and D. B. Sinars, Phys. Plasmas **23**, 012705 (2016).

[30] M. Geissel, T. J. Awe, D. E. Bliss, M. E. Campbell, M. R. Gomez, E. Harding, A. J. Harvey-Thompson, S. B. Hansen, C. Jennings, M. W. Kimmel, P. Knapp, S. M. Lewis, R. D. McBride, K. Peterson, M. Schollmeier, D. J. Scoglietti, A. B. Sefkow, J. E. Shores, D. B. Sinars, S. A. Slutz, I. C. Smith, C. S. Speas, R. A. Vesey, and J. L. Porter, Proc. SPIE **9731**, 97310O (2016).

[31] M. R. Gomez, S. A. Slutz, A. B. Sefkow, K. D. Hahn, S. B. Hansen, P. F. Knapp, P. F. Schmit, C. L. Ruiz, D. B. Sinars, E. C. Harding, C. A. Jennings, T. J. Awe, M. Geissel, D. C. Rovang, I. C. Smith, G. A. Chandler, G. W. Cooper, M. E. Cuneo, A. J. Harvey-Thompson, M. C. Herrmann, M. H. Hess, D. C. Lamppa, M. R. Martin, R. D. McBride, K. J. Peterson, J. L. Porter, G. A. Rochau, M. E. Savage, D. G. Schroen, W. A. Stygar, and R. A. Vesey, Phys. Plasmas **22**, 056306 (2015).